sustainability

MDPI

Article

Research on the Effect of Hazard Visibility on Drivers' Avoidance Behavior and Discriminant Model

Jing Zhang [1], Yujia Hou [1] and Tianzheng Wei [2,*]

[1] Transportation Bureau of Bincheng District, Binzhou 256602, China; 18854358099@163.com (J.Z.); houyujiah@163.com (Y.H.)
[2] School of Transportation and Logistics Engineering, Shandong Jiaotong University, Jinan 250357, China
* Correspondence: weitianzheng@sdjtu.edu.cn

Abstract

To investigate the effects of hazard visibility on drivers' avoidance behaviors and safety risks, this study developed driving scenarios involving overt and covert hazards using a high-fidelity driving simulator and conducted a series of driving experiments. A linear mixed model (LMM) was employed to systematically examine the variations in vehicle kinematic characteristics, operational response behaviors, and collision risks under different hazard visibility conditions. Furthermore, a driver avoidance capability classification model was developed by integrating factor analysis with Bayesian linear discriminant analysis. The results showed that hazard visibility was a critical factor influencing drivers' responses. Compared with overt hazards, covert hazards significantly reduced time to collision (TTC) and increased the maximum braking pedal force of the driver. The driver avoidance capability classification model achieved an accuracy of 85.8%, enabling effective identification of drivers with low, medium, and high avoidance capabilities. These findings provide insights into driver avoidance behavior and may support driver safety assessment and traffic safety education, with potential implications for reducing crash-related injuries and economic losses, as well as promoting the sustainable development of transportation.

Keywords: traffic safety; driving behavior; factor analysis; linear discrimination; traffic sustainability

1. Introduction

With the continuous growth of the global vehicle fleet and the increasing complexity of road traffic environments, traffic accidents have become a critical threat to human safety and property security [1]. Previous studies have demonstrated that driver-related factors represent one of the primary contributors to traffic accidents, among which driving errors, traffic violations, and insufficient identification and assessment of potential traffic risks are major causes of crash occurrence [2–4]. In driving environments, risk events are characterized by their suddenness, dynamic evolution, and strong contextual dependence, requiring drivers to continuously perceive surrounding traffic conditions and rapidly perform risk assessment and behavioral decision-making [5,6]. However, due to individual differences in drivers' perceptual capabilities, cognitive workload, and decision-making strategies, the processes of risk perception and behavioral decision-making exhibit substantial uncertainty and nonlinear characteristics [7]. When drivers fail to detect potential hazards in time and adopt appropriate and effective avoidance maneuvers, traffic accidents will occur, resulting in severe human casualties and economic losses [8]. Therefore, a comprehensive investigation of driver avoidance behavior characteristics and the development of reliable avoidance

Check for updates

Academic Editor: Jinjun Tang

Received: 1 August 2026
Revised: 29 September 2026
Accepted: 18 October 2026
Published: 28 October 2026

Copyright: © 2026 by the authors. Licensee MDPI, Basel, Switzerland. This article is an open access article distributed under the terms and conditions of the Creative Commons Attribution (CC BY) license.

capability classification models are of considerable theoretical and practical significance for traffic safety management, driver training and assessment, and the advancement of intelligent driving assistance systems, which is an essential prerequisite for realizing the sustainable development of road traffic systems.

In potential crash risk scenarios, driving behavior data provide direct information for identifying hazardous states [9]. Variables such as vehicle speed, longitudinal and lateral acceleration, braking and steering inputs, lane position deviation, and relative distance and relative velocity to the preceding vehicle can characterize drivers' control strategies and risk mitigation responses from multiple perspectives [10]. Previous studies have demonstrated that drivers may exhibit substantial individual differences in emergency responses under identical critical driving conditions, with braking and steering reaction times varying by severalfold. Moreover, approximately 80% of drivers tend to take braking rather than steering maneuvers when responding to imminent hazards [11]. However, behavioral variables alone are insufficient to fully capture the progression of collision risk and the severity of traffic conflicts. Therefore, surrogate safety measures (SSM) have been widely introduced to quantitatively characterize traffic risks [12]. Compared with traditional indicators such as vehicle speed and time headway, time to collision (TTC) directly represents the remaining time before a potential collision occurs and provides an intuitive measure of temporal urgency in hazardous situations. Consequently, TTC has been extensively applied in rear-end conflict analysis, risk stratification, and hazardous event identification, serving as an essential criterion for risk level classification and the determination of appropriate avoidance timing [13–16].

Hazard visibility refers to the degree of difficulty with which a hazard is exposed and can be directly perceived by humans or detected by sensing devices. It represents a critical prerequisite influencing drivers' emergency avoidance decision-making [17]. Previous studies have demonstrated that drivers' hazard perception is often characterized by delays and incompleteness, and such perceptual differences directly determine the available response time and operational space for subsequent avoidance maneuvers [18]. Hazard visibility can generally be categorized into overt hazards and covert hazards [19,20]. Overt hazards refer to hazard sources that can be directly identified by drivers through visual observation, such as pedestrians walking on the roadway or vehicles ahead activating brake lights. Due to their high detectability, overt hazards can typically be recognized promptly, allowing drivers to initiate immediate avoidance responses, such as deceleration or lane changing. In contrast, covert hazards refer to hazard sources that are partially or completely obscured by other road users or environmental factors. These hazards are not readily observable by drivers and require them to rely on their driving experience or to actively gather information from the surrounding traffic environment. Therefore, drivers need to detect the presence of covert hazards as early as possible and proactively prepare appropriate avoidance strategies to mitigate potential collision risks.

Regarding driver avoidance capability classification, Bayesian methods have been widely applied in the identification of risky driving behaviors due to their robust classification performance and probabilistic interpretation capability [21–23]. For instance, previous studies have developed Bayesian network-based models for identifying hazardous driving behaviors and employed sensitivity analysis to reveal the underlying relationships between influencing factors and driving risk [22]. Other studies have applied Bayesian classifiers to driving simulator data for risk scoring, achieving effective differentiation between aggressive and safe driving styles [24]. However, most studies directly incorporate behavioral variables into Bayesian models, with limited consideration of the potential influence of multicollinearity among variables on classification performance. As an effective dimensionality reduction technique, factor analysis can extract representative common factors from

a set of highly correlated variables, thereby uncovering the latent structures underlying avoidance behaviors [25–27]. Integrating factor analysis with Bayesian linear discriminant analysis can not only mitigate the adverse effects of multicollinearity but also improve the scientific validity and interpretability of classification outcomes. Nevertheless, there remains a gap in research that combines factor analysis and Bayesian linear discriminant analysis for identifying driver avoidance capability from the perspective of hazard visibility.

Although previous studies have provided important foundations for the identification of risky driving behaviors and the assessment of traffic hazards, many investigations have focused primarily on specific risk scenarios or crash-prone situations. Limited attention has been paid to drivers' behavioral responses under overt hazard and covert hazard conditions, and the coupling relationships between driving behavior characteristics and risk-related indicators remain insufficiently understood. To address these gaps, this study investigates driver avoidance behavior from the perspective of hazard visibility. Based on TTC, driving risk was categorized into three levels: low, medium, and high risk. A driving simulator experiment was conducted to collect drivers' avoidance behavior data under different hazard scenarios. Factor analysis was first applied to reduce the dimensionality of the behavior variables and extract common factors representing comprehensive driver avoidance capability. Subsequently, Bayesian linear discriminant analysis was employed to develop a driver avoidance capability classification model, enabling effective identification and classification of drivers with different levels of avoidance capability. The findings of this study contribute to a deeper understanding of the underlying mechanisms and individual differences in driver avoidance behaviors under varying hazard visibility conditions. Furthermore, the proposed approach provides theoretical insights and methodological support for quantitative assessment of driver hazard perception capability, the development of hierarchical driver training programs, and the optimization of warning strategies in intelligent driving assistance systems, which is conducive to further improving traffic safety and promoting sustainable transportation development.

2. Methodology

2.1. Participants

To ensure the validity and consistency of the experimental data, all recruited participants were required to hold a valid C1 driving license, have normal or corrected-to-normal vision, and maintain a good physical and psychological condition during the experiment without any factors that could impair their driving ability. To minimize potential interference from alcohol or medication, participants were instructed to abstain from alcohol consumption within 24 h before the experiment and avoid taking any medication that could affect driving performance or cognitive function. A total of 39 drivers were recruited for this study. During the experiment, two participants experienced discomfort, such as dizziness, and were unable to complete the assigned tasks. Consequently, data from 37 participants who successfully completed all hazardous test scenarios were retained for subsequent analysis. Among these participants, 22 were male, and 15 were female. The driving experience ranged from 1 to 16 years, with a mean of 3.89 years and a standard deviation of 3.85 years. Their age ranged from 20 to 45 years, with a mean of 26.51 years and a standard deviation of 7.07 years.

2.2. Apparatus

This study employed a driving simulator platform developed based on SCANeR Studio V1.8, which integrates a virtual simulation system, a data acquisition system, and a driving simulation system. The driving simulation system consisted of a manual-transmission Volkswagen sedan with a length of 4.6 m, an 180° wraparound projection screen, and

two computers for equipment control, as illustrated in Figure 1. The virtual simulation system was developed using SCANeR Studio, which supports Python language-based scenario scripting and enables precise control of event-triggering locations and timings through the MICE scripting language. This capability allows the implementation of high-risk events, such as unexpected pedestrian crossings and sudden braking by preceding vehicles, with accurate temporal and spatial control. SCANeR Studio also provides integrated data acquisition and analysis modules, enabling real-time recording and synchronized storage of multimodal data collected during simulated driving. The built-in analysis module facilitates the extraction of vehicle dynamics and driver operation data. The hardware configuration of the data acquisition system included 16 analog input channels, 24-bit analog-to-digital conversion accuracy, two general-purpose switch signal channels, eight counting input channels, one CAN communication channel, and a GPS synchronization module. The system recorded experimental data at a sampling frequency of 100 Hz, ensuring the temporal continuity and spatial consistency of vehicle dynamic parameters.



Figure 1. Driving simulator.

2.3. Experimental Scenarios

This study developed an urban roadway environment consisting of four bidirectional six-lane roads connected by intersections to ensure smooth transitions between experimental scenarios. Each lane was designed with a width of 3.25 m and a speed limit of 60 km/h. Lane separation markings were represented by 15-cm-wide white dashed lines, while lane edge markings were represented by white solid lines of the same width. The surrounding environment was constructed with road surfaces, roadside trees, streetlights, and buildings, and traffic signals were installed at intersections. At each intersection, pedestrian crosswalk markings were provided, along with a 30-cm-wide stop line located 3 m upstream of the crosswalk. In addition, pedestrian warning signs and roadwork warning signs were placed 50 m upstream of the corresponding crosswalks and construction areas, respectively. Considering different hazard source types, multiple traffic conflict scenarios were developed. Hazard sources were categorized into two types: overt hazards and covert hazards. The conflicting objects were classified into three categories: vehicle–vehicle conflicts (V-V), vehicle–cycle conflicts (V-C), and vehicle–pedestrian conflicts (V-P). As presented in Table 1, seven scenarios were designed in this study, including three non-conflict scenarios (distracting event). In each scenario, the occurrence time and trajectory changes of events are determined by setting action trigger points on the driving path of the test vehicle. When the test driver triggers this action control point during driving, the actions of surrounding

vehicles or pedestrians are activated, and the scene simulation will be completed according to the preset actions and directions.

Table 1. Description of hazardous events.

Number	Hazard Visibility	Conflicting Objects	Description of Traffic Conflict Scenarios
1	Distracting event	V-V	The test vehicle was travelling in the middle lane, with a sedan moving forward in the same direction on the front right side of the same lane.
2	Distracting event	V-C	The test vehicle was travelling in the middle lane, with a cyclist riding forward on its front right side.
3	Distracting event	V-P	The test vehicle was approaching the intersection, while a pedestrian walked along the roadside on the right in the same travelling direction.
4	Overt hazard	V-P	The test vehicle approached the intersection with the intention of passing straight through under a green signal for the through movement. At that moment, a child waiting to cross the street at the crosswalk on the roadside suddenly ran across to the opposite side of the road.
5	Overt hazard	V-V	A heavy-duty truck was travelling in the same direction ahead. Blocked by the leading vehicle, the test vehicle failed to obtain a clear view of the road conditions ahead. During normal cruising, the preceding truck abruptly applied emergency braking.
6	Covert hazard	V-V	The test vehicle was travelling in the middle lane and intended to proceed straight through the intersection with a green through signal. A construction zone shielded by isolation barriers was located at the intersection, and a roadwork warning sign was placed 50 m in advance of the construction area. Meanwhile, a sedan was about to exit from behind the isolation barriers.
7	Covert hazard	V-P	The bus stopped at the right-side bus stop located on the front right side of the test vehicle. As the test vehicle approached, a pedestrian suddenly emerged from the front of the bus and attempted to cross the roadway.

2.4. Procedure

Before the experiment, basic demographic information of each participant was collected to characterize individual driver attributes.

The physical and psychological conditions of participants were assessed to ensure that they maintained normal cognitive functioning and driving capability and met the experimental requirements. Participants were then provided with a detailed introduction to the driving simulator, including its basic functions, vehicle control operations, experimental objectives, procedures, and safety precautions. The operational requirements and safety instructions during the experiment were clearly explained to ensure that participants fully understood the experimental tasks and procedures.

Before the formal trials, participants completed an adaptive driving training session in a predefined practice scenario. The training covered fundamental driving operations, including vehicle starting, acceleration and deceleration, braking, steering, and lane changing.

After completing the adaptation training, participants were provided with a resting period of approximately 10 min to alleviate the cognitive workload and visual fatigue induced by initial simulator exposure. The formal experiment was initiated only after participants returned to a relatively stable driving state.

During the formal experiment, participants were instructed to complete the predefined driving tasks according to their driving habits while strictly complying with traffic regulations. If a collision occurred during the experiment, the simulator maintained the vehicle dynamics model and motion state unchanged, and participants continued the subsequent driving tasks to ensure the completeness of data collection for each hazard scenario. Each participant completed all hazard scenarios in a single formal trial, with each trial lasting approximately 6 min.

After completion of the formal experiment, the collected data were examined by the experimenters for integrity and validity before storage. Participants who completed the experiment will receive a monetary reward.

2.5. Data Processing

The driving simulator recorded vehicle and driver data at a sampling frequency of 100 Hz. For each hazard scenario, data collected from 120 m upstream of the potential collision conflict point to the conflict point were extracted for analysis [28]. Based on the coordinate trajectories of drivers in each experimental scenario, the corresponding simulator data were identified and filtered, and the complete driving data from all participants across all scenarios were obtained. To comprehensively characterize drivers' behavioral responses under hazard conditions, this study extracted driving behavior variables from vehicle motion states, driver operational states, and driver response states.

Vehicle motion-related variables included the speed, acceleration, maximum deceleration, and initial braking speed. These variables characterize the vehicle's dynamic operating state and indirectly reflect drivers' control strategies, thereby serving as important indicators for evaluating driving risk levels.

Driver control-related variables included the maximum steering wheel rotation angle, the brake pedal force (BPF), and the maximum brake pedal force (Max BPF). Drivers typically perform evasive maneuvers through braking and steering adjustments [29]. The steering wheel rotation magnitude and brake pedal force applied during emergency braking reflect drivers' perceived urgency when responding to hazards and reveal individual differences in avoidance capability.

Response-related variables included brake reaction time (BRT) and braking response position (BRP). BRT was defined as the time interval between the onset of the hazard event and the moment when the driver initiated braking. Braking response position was defined as the distance traveled by the vehicle from the starting point of the hazard scenario to the moment when braking was initiated. These two indicators characterize drivers' response speed under hazardous traffic conditions and provide a more detailed representation of individual differences in avoidance capability.

In hazard scenarios, a collision with the target object would occur if drivers failed to initiate braking within a certain period. Therefore, the moment at which drivers performed an effective avoidance response was defined as the onset of the traffic conflict. The TTC value, representing the level of collision risk, was calculated by dividing the distance between the vehicle and the expected collision point at conflict onset by the vehicle speed at that moment.

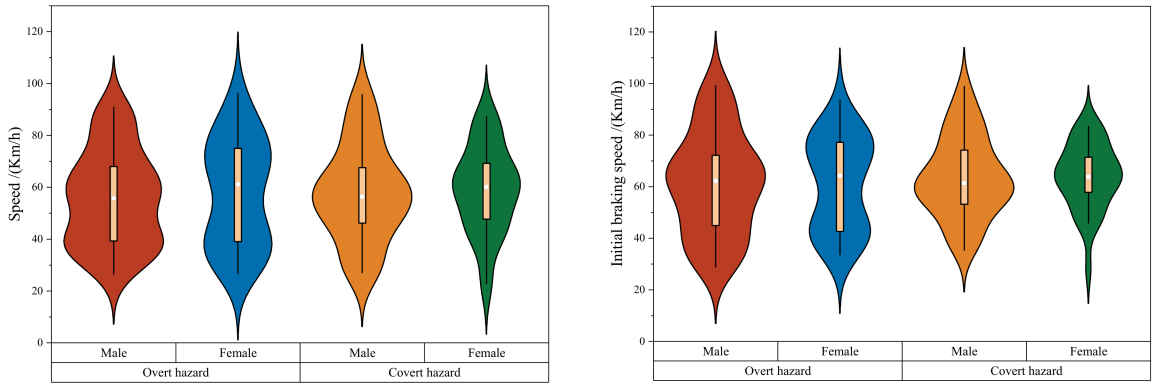
3. Results

3.1. Analysis of Influence Factors

To investigate the effects of driver gender and hazard visibility on vehicle motion characteristics, a linear mixed model (LMM) was conducted to examine their effects on vehicle speed, acceleration, maximum deceleration, and initial braking speed under hazardous conditions. The normality assumption of the LMM was verified using the Shapiro–Wilk test on standardized residuals. The results showed that the standardized residuals approximately followed a normal distribution ($p > 0.05$), and residual variance was homogeneous, satisfying the assumptions of the LMM.

The results of the LMM indicated that the interaction effect between driver gender and hazard visibility on vehicle speed was not statistically significant ($F(1,148) = 0.037$, $p = 0.848 > 0.05$). The simple main effects analysis further demonstrated that neither driver gender ($F(1,148) = 0.175$, $p = 0.678 > 0.05$) nor hazard visibility ($F(1,148) = 0.410$, $p = 0.523 > 0.05$) had a significant effect on vehicle speed. Similarly, the interaction effect between driver gender and hazard visibility on initial braking speed was not significant ($F(1,148) = 0.006$, $p = 0.938 > 0.05$). The simple main effects analysis showed that neither driver gender ($F(1,148) = 0.001$, $p = 0.970 > 0.05$) nor hazard visibility ($F(1,148) = 1.207$, $p = 0.274 > 0.05$) significantly influenced initial braking speed.

At the onset of braking, most drivers maintained their vehicle speeds at approximately 60 km/h in accordance with the speed limit, as shown in Figure 2, although some participants exceeded the speed limit. The mean driving speeds exhibited only minor differences across different hazard scenarios.



(**a**) Speed (**b**) Initial braking speed

Figure 2. Speed distribution.

The LMM results indicated that the interaction effect between driver gender and hazard visibility on acceleration was not statistically significant ($F(1,148) = 0.337$, $p = 0.562 > 0.05$). Neither driver gender ($F(1,148) = 0.027$, $p = 0.870 > 0.05$) nor hazard visibility ($F(1,148) = 3.267$, $p = 0.073 > 0.05$) exhibited a significant main effect on acceleration. As illustrated by the violin boxplots of vehicle acceleration distributions under different hazard visibility and driver genders (Figure 3), male and female drivers showed similar acceleration distribution patterns, although males exhibited slightly higher median acceleration values than females. Furthermore, covert hazards induced stronger deceleration responses among all drivers, resulting in an overall shift in acceleration distributions toward the negative range.

The interaction effect between driver gender and hazard visibility on maximum deceleration was not statistically significant ($F(1,148) = 0.346$, $p = 0.557 > 0.05$). Similarly, neither driver gender ($F(1,148) = 0.028$, $p = 0.868 > 0.05$) nor hazard visibility ($F(1,148) = 3.358$,

$p = 0.069 > 0.05$) showed a significant main effect on maximum deceleration. As illustrated by the violin boxplots of maximum deceleration distributions for different hazard visibility and driver genders (Figure 4), male drivers exhibited a higher mean maximum deceleration than female drivers. Compared with covert hazard scenarios, drivers under overt hazard scenarios showed lower maximum deceleration values across both genders, accompanied by a more pronounced bimodal distribution pattern. In contrast, covert hazard scenarios induced drivers to adopt stronger braking responses, characterized by greater maximum braking deceleration.

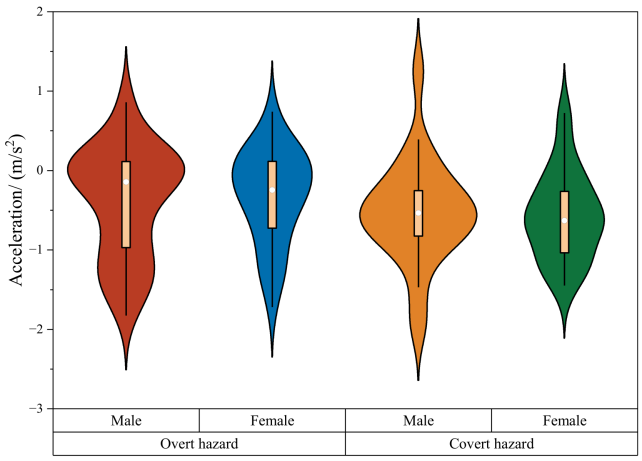


Figure 3. Acceleration.

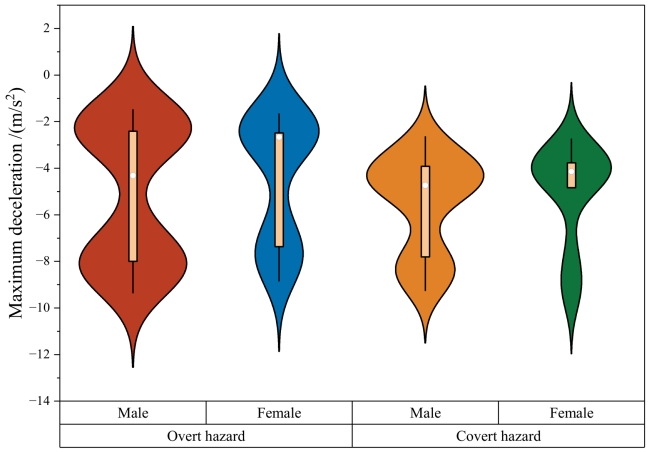


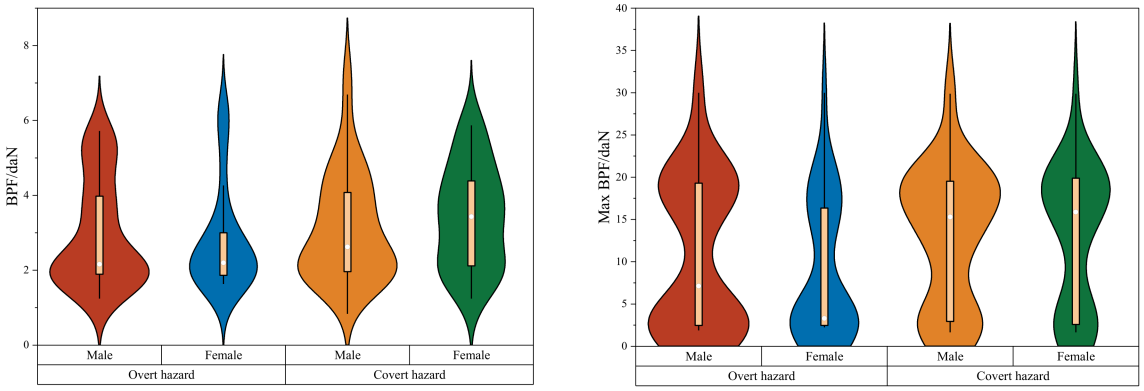
Figure 4. Maximum deceleration.

To investigate the effects of driver gender and hazard visibility on driver control inputs, the LMM was conducted to examine their effects on the maximum steering wheel rotation angle, BPF, and Max BPF under hazardous conditions. For the analysis of maximum steering wheel rotation angle, an absolute single steering angle change greater than 5° was defined as an active steering maneuver initiated by the driver. Statistical analysis of the maximum steering wheel rotation angle during hazard scenarios revealed that the majority of drivers relied solely on braking to avoid potential collisions under critical collision-imminence conditions, whereas only 18.2% of drivers selected abrupt steering maneuvers as an avoidance strategy.

The LMM was conducted to investigate the effects of driver gender and hazard visibility on BPF. The results indicated that the interaction effect between gender and hazard visibility was not statistically significant ($F(1,148) = 1.052$, $p = 0.307 > 0.05$). Neither driver gender ($F(1,148) = 0.056$, $p = 0.814 > 0.05$) nor hazard visibility ($F(1,148) = 2.758$, $p = 0.100 > 0.05$)

showed a significant main effect on BPF. Similarly, the interaction effect between gender and hazard visibility on Max BPF was not significant ($F(1,148) = 0.449$, $p = 0.504 > 0.05$), and driver gender had no significant effect on Max BPF ($F(1,148) = 0.497$, $p = 0.486 > 0.05$). However, hazard visibility exerted a significant effect on Max BPF ($F(1,148) = 5.254$, $p = 0.024 < 0.05$, $\eta_p^2 = 0.034$). Pairwise comparisons revealed that drivers under covert hazard conditions exhibited significantly greater Max BPF than those under overt hazard conditions, with a mean difference of 3.186 daN (95% confidence interval is 0.431–5.940 daN).

The violin boxplots of BPF and Max BPF are presented in Figure 5. A comparison of the distributions showed that under overt hazard conditions, male drivers exhibited higher median values of both BPF and Max BPF than female drivers, indicating stronger emergency braking inputs. In contrast, under covert hazard conditions, female drivers increased their braking pedal force and exceeded male drivers in BPF. Meanwhile, the difference in Max BPF distributions between male and female drivers became substantially reduced, suggesting that both genders adopted high-intensity braking strategies when responding to suddenly emerging covert hazards.



(**a**) BPF (**b**) Max BPF

Figure 5. Brake pedal force.

To investigate the effects of driver gender and hazard visibility on driver response characteristics, the LMM was conducted to examine their effects on BRT and BRP under hazardous conditions. The results indicated that the interaction effect between driver gender and hazard visibility was not statistically significant for either BRT ($F(1,148) = 0.384$, $p = 0.537 > 0.05$) or BRP ($F(1,148) = 0.267$, $p = 0.606 > 0.05$). The simple main effects analysis further showed that neither driver gender ($F(1,148) = 1.153$, $p = 0.290 > 0.05$) nor hazard visibility ($F(1,148) = 2.660$, $p = 0.106 > 0.05$) had a significant effect on BRT. As shown in Figure 6, drivers exhibited longer average BRT under covert hazard conditions than under overt hazard conditions. Under overt hazard conditions, female drivers demonstrated a significantly lower median BRT than male drivers, indicating faster hazard recognition and braking initiation responses, with a more concentrated distribution of response times. In contrast, under covert hazard conditions, female drivers showed increased BRT, while the differences between male and female drivers in terms of median BRT, interquartile range, and overall distribution characteristics became significantly reduced.

Driver gender had no significant effect on BRP ($F(1,148) = 0.302$, $p = 0.586 > 0.05$). However, hazard visibility exhibited a significant effect on braking response position ($F(1,148) = 8.895$, $p < 0.01$, $\eta_p^2 = 0.057$). Pairwise comparisons revealed that drivers under covert hazard conditions initiated braking at a significantly later position than those under overt hazard conditions, with a mean difference of 11.762 m (95% confidence interval

is 3.946–19.579). As shown in Figure 7, under overt hazard conditions, male drivers exhibited higher median BRP values than female, indicating that they initiated braking later and maintained a smaller safety margin before collision. In addition, male drivers showed a lower degree of data dispersion. Under covert hazard conditions, BRP values increased for both male and female drivers, with female drivers exhibiting higher median BRP values than males. Meanwhile, the overall distribution patterns of BRP between the two genders became increasingly similar.

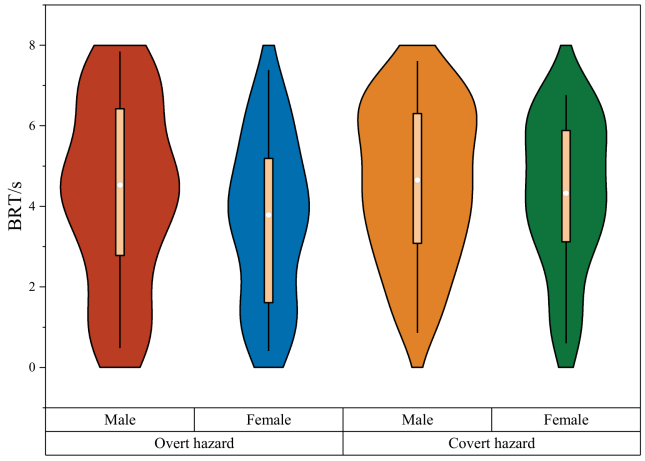


Figure 6. Braking response time.

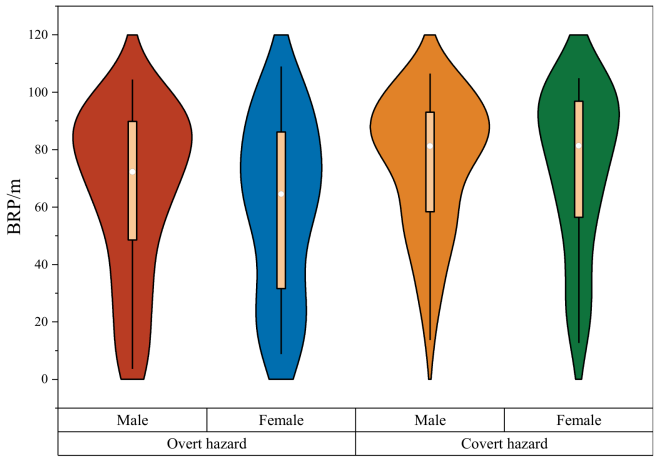


Figure 7. Braking response position.

The interaction effect between driver gender and hazard visibility on TTC was not statistically significant ($F(1,148) = 0.122$, $p = 0.727 > 0.05$), and driver gender showed no significant effect on TTC ($F(1,148) = 0.390$, $p = 0.536 > 0.05$). However, hazard visibility had a significant effect on TTC ($F(1,148) = 15.362$, $p < 0.01$, $\eta_p^2 = 0.094$). Pairwise comparisons revealed that drivers under covert hazard conditions exhibited significantly lower TTC values than those under overt hazard conditions, with a mean difference of 0.922 s (95% confidence interval is 0.456–1.388 s). As shown in Figure 8, covert hazards substantially reduced drivers' temporal safety margins before potential collisions. Under both overt and covert hazard conditions, female drivers exhibited higher mean TTC values than male drivers, indicating greater collision avoidance redundancy and a larger available safety margin.

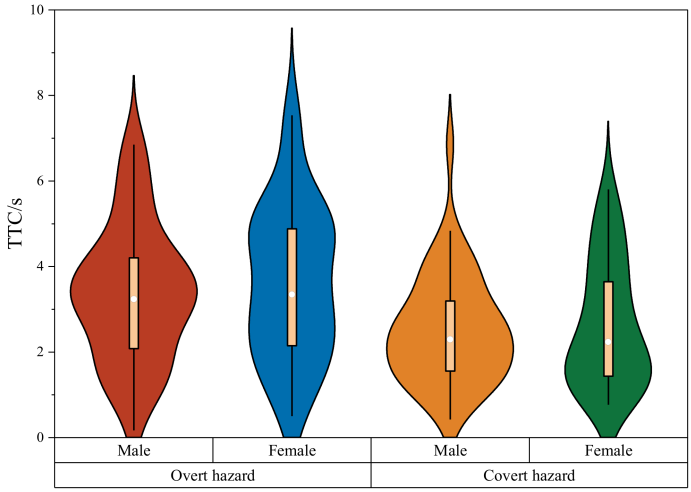


Figure 8. TTC.

3.2. Correlation Analysis

To investigate the relationships among the variables, Spearman correlation analysis was used. The results are presented in Figure 9. Significant correlations were observed between TTC and all investigated variables, including BPF, Max BPF, acceleration, maximum deceleration, speed, initial braking speed, BRT, and BRP. Drivers with stronger avoidance capability generally exhibited lower BPF, Max BPF, and maximum deceleration in terms of control behavior, indicating that they could effectively avoid potential collisions with less intensive braking inputs. Regarding vehicle motion characteristics, stronger avoidance capability was associated with lower speed and acceleration, suggesting more cautious vehicle control strategies. In terms of response characteristics, stronger avoidance capability was reflected by shorter BRT and smaller BRP values, indicating that these drivers were able to perceive potential collision risks earlier and initiate braking with shorter response delays and greater remaining distance from the conflict point.

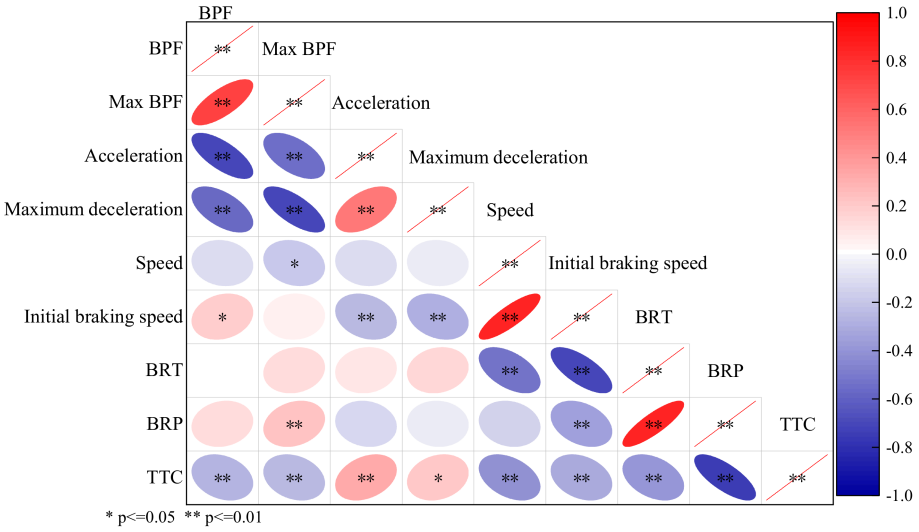


Figure 9. Correlation Analysis.

As shown in Figure 9, strong correlations existed among the investigated variables, indicating substantial information redundancy among these indicators. To reduce data complexity and improve the efficiency of subsequent analysis, factor analysis was employed to simplify the dataset and extract representative latent factors.

3.3. Data Dimension Reduction Based on Factor Analysis

Factor analysis is a widely used dimensionality reduction technique. Its fundamental concept is to identify groups of observed variables with strong interrelationships by analyzing the correlation structure among variables, and to represent the primary information contained within these variable groups using a smaller number of latent variables [30]. These latent variables, which capture the common characteristics shared among the original variables, are referred to as common factors. By extracting common factors, factor analysis can reduce the dimensionality of the dataset while preserving the essential information contained in the original variables. However, because common factors can only explain part of the shared variance among observed variables, some information cannot be fully represented by the common factors. This unexplained portion is generally defined as specific factors or unique factors.

Let the random variable vector be $X = (X_1, X_2, ..., X_p)$. The general formulation of the factor analysis model is expressed as Equation (1).

$$X_i = \alpha_{i1}F_1 + \alpha_{i2}F_2 + ... + \alpha_{im}F_m + \varepsilon_i, \quad (i = 1, 2, ..., p) \tag{1}$$

In Equation (1), $F_1, F_2, ..., F_m$ represent the common factors, and ε_i denotes the unique factor, which accounts for the influence of variables not explained by the common factors, where $m \leq p$. The matrix representation of the factor analysis model is given in Equation (2).

$$\mathrm{X} = \mathrm{AF} + \varepsilon \tag{2}$$

where

$$X = \begin{bmatrix} X_1 \\ X_2 \\ \vdots \\ X_P \end{bmatrix}, \ \mathrm{A} = \begin{bmatrix} \alpha_{11} & \alpha_{12} & \cdots & \alpha_{1m} \\ \alpha_{21} & \alpha_{22} & \cdots & \alpha_{2m} \\ \cdots & \cdots & \cdots & \cdots \\ \alpha_{p1} & \alpha_{p2} & \cdots & \alpha_{pm} \end{bmatrix}, \ \mathrm{F} = \begin{bmatrix} F_1 \\ F_2 \\ \vdots \\ F_P \end{bmatrix}, \ \varepsilon = \begin{bmatrix} \varepsilon_1 \\ \varepsilon_2 \\ \vdots \\ \varepsilon_P \end{bmatrix} \tag{3}$$

Matrix A represents the factor loading matrix. The loading of the *i*-th observed variable on the *j*-th factor is denoted by the coefficient α_{ij}, which reflects the contribution of variable X_i to the corresponding common factor $\mathrm{F_j}$.

Factor analysis was performed to reduce the dimensionality of behavioral indicators, including BPF, Max BPF, acceleration, maximum deceleration, speed, initial braking speed, BRT, and BRP. The results showed that the Kaiser–Meyer–Olkin (KMO) measure of sampling adequacy was 0.645, which is mediocre but exceeds the recommended threshold of 0.5, indicating that the dataset was suitable for factor analysis [31]. In addition, Bartlett's test of sphericity yielded a *p*-value below the significance level of 0.01, leading to the rejection of the null hypothesis that the correlation matrix is an identity matrix. This result confirmed the existence of significant correlations among the investigated variables, further demonstrating the suitability of applying factor analysis to the dataset.

As shown in Table 2, all values in the Extraction column exceeded 0.7, indicating that more than 70% of the variance of each original variable could be explained by the extracted common factors. This result suggests that the extracted factors effectively captured the majority of information contained in the original variables.

As shown in Table 3, three factors with eigenvalues greater than 1 were successfully extracted. The cumulative variance contribution rate of these three factors reached 86.68%, indicating that the extracted common factors accounted for the majority of the variance contained in the original variables.

Table 2. Variance of Common Factors.

Variable	Original	Extraction
BPF	1.00	0.83
Max BPF	1.00	0.85
Acceleration	1.00	0.70
Maximum deceleration	1.00	0.70
Speed	1.00	0.97
Initial braking speed	1.00	0.94
BRT	1.00	0.97
BRP	1.00	0.98

Table 3. Variance Contribution Rate.

Component	Initial Feature Value			Sum Squares of the Loads			Rotational Load Sum of Squares		
	Total	Percentage of Variance	Cumulative Percentage	Total	Percentage of Variance	Cumulative Percentage	Total	Percentage of Variance	Cumulative Percentage
1	3.11	38.89	38.89	3.11	38.89	38.89	3.04	38.05	38.05
2	2.79	34.85	73.74	2.79	34.85	73.74	2.03	25.36	63.41
3	1.03	12.94	86.68	1.03	12.94	86.68	1.86	23.26	86.68
4	0.50	6.26	92.93						
5	0.30	3.80	96.73						
6	0.15	1.89	98.62						
7	0.07	0.83	99.44						
8	0.04	0.56	100.00						

To improve the interpretability of the common factors, the factor loading matrix was rotated using the maximum variance method, and the rotated factor loading matrix is presented in Table 4. The results show that BPF, Max BPF, acceleration, and maximum deceleration exhibited relatively high loadings on Factor 1 (F_1), indicating that this factor primarily represents drivers' control characteristics. Therefore, Factor 1 was defined as the control factor.

Table 4. Factor loading matrix after rotation.

Variable	Common Factor		
	F_1	F_2	F_3
BPF	0.91	−0.05	0.02
Max BPF	0.90	−0.10	0.15
Maximum deceleration	−0.82	−0.11	0.07
Acceleration	−0.80	−0.21	−0.06
Speed	−0.07	0.98	−0.08
Initial braking speed	0.23	0.88	−0.35
BRP	0.15	−0.05	0.98
BRT	−0.03	−0.47	0.86

Speed and initial braking speed showed relatively high loadings on Factor 2 (F_2), suggesting that this factor mainly reflects vehicle speed-related characteristics. Accordingly, Factor 2 was defined as the speed factor. In addition, BRT and BRP exhibited relatively high loadings on Factor 3 (F_3), indicating that this factor captures drivers' response characteristics. Therefore, Factor 3 was defined as the driver response factor. It is worth explaining that the rotated factor loading matrix showed that BRT had a primary loading of 0.86 on Factor 3 and a secondary loading of −0.47 on Factor 2. This represents mild cross-loading, as the secondary loading exceeds the absolute value of 0.4. BRT is primarily interpreted as an indicator of Factor 3.

3.4. Driver Avoidance Capability Discrimination Model

The potential collision risk was categorized into three levels based on TTC thresholds of 2 s and 3.5 s [32,33], which were used to characterize drivers' avoidance capability. Specifically, TTC < 2 s was defined as a high potential collision risk level, corresponding to a low avoidance capability level. A TTC value ranging from 2 s to less than 3.5 s (2 s ≤ TTC < 3.5 s) represented a moderate collision risk level, corresponding to a medium avoidance capability level. TTC ≥ 3.5 s indicated a relatively low collision risk level, corresponding to a high avoidance capability level. The classification results are presented in Figure 10.

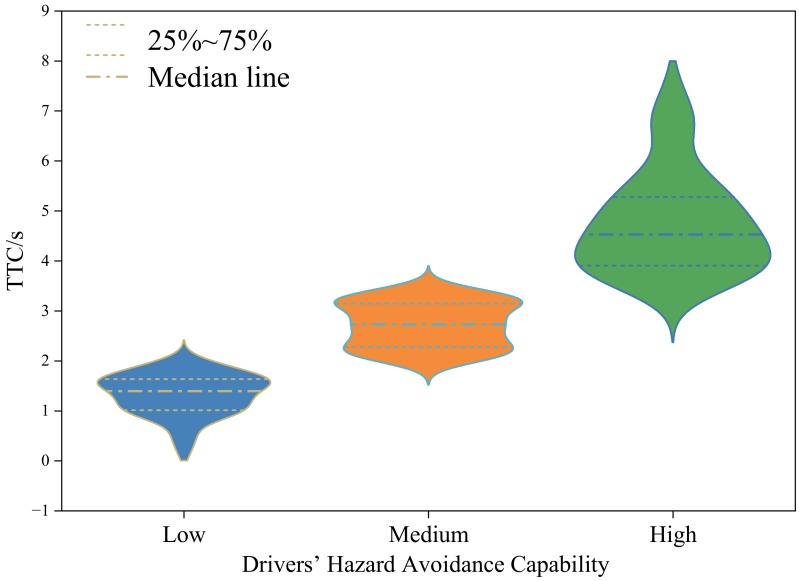


Figure 10. TTC violin diagram.

The Bayesian linear discriminant method is a probabilistic classification approach based on discriminant analysis [34]. Assume that there are k populations, denoted as G_1, G_2, ..., G_k. Calculate the conditional probability P(G = i|X = x), where i = 1, 2, ..., k, that the sample belongs to each population. Let $f_i(x)$ and Πi represent the conditional probability density function and prior probability of population G = i, respectively. Similarly, $f_j(x)$ and Π_j denote the conditional probability density function and prior probability of population G = j. By calculating the posterior probabilities of the sample under all k possible populations and comparing their values, the sample is assigned to the population with the highest posterior probability. The Bayesian linear discriminant function is expressed as Equation (4).

$$P(G = i \mid X = x) = \frac{P(X \mid G)P(G)}{P(X)} = \frac{f_i(x)\Pi_i}{\sum_{j=1}^{k} f_j(x)\Pi_j},\ i = 1, 2, \ldots, k \tag{4}$$

Assuming that X follows a D-dimensional normal distribution, μ_i represents the mean vector of the i-th class distribution, and Σ denotes the pooled within-class covariance matrix shared across all groups, as expressed in Equation (5).

$$f_i(x) = \frac{1}{(2\Pi)^{\frac{D}{2}}|\Sigma|^{\frac{1}{2}}} \exp\left\{-\frac{1}{2}(x-\mu_i)^T\Sigma^{-1}(x-\mu_i)\right\} \tag{5}$$

When P(G = i|X = x) = maxP(G = j|X = x), where 1 ≤ j ≤ k, the sample x is assigned to class i.

In this study, driver gender, hazard visibility, and the three common factors extracted through factor analysis were used as input variables for Bayesian linear discriminant analysis

to develop a driver avoidance capability discrimination model. Two canonical discriminant functions were constructed. The first canonical discriminant function had an eigenvalue of 4.031 and accounted for 98.3% of the total variance, whereas the second canonical function explained the remaining 1.7%. Wilks' Lambda test results showed that both discriminant functions were statistically significant ($p < 0.05$), indicating that the developed discriminant functions had strong discriminatory power and could effectively distinguish samples among different avoidance capability categories.

Based on the weighting coefficients of the original variables in the two discriminant functions, the corresponding discriminant functions were established as shown in Equation (6).

$$\begin{aligned} g_1 &= 0.092x_1 - 0.020x_2 + 0.758F_1 + 0.948F_2 + 1.249F_3 \\ g_2 &= 0.521x_1 + 0.041x_2 + 0.784F_1 - 0.216F_2 - 0.150F_3 \end{aligned} \quad (6)$$

where x_1 and x_2 represent driver gender (1 for male and 2 for female) and hazard visibility (1 for covert hazard and 2 for overt hazard), respectively. According to the standardized coefficient equations in Equation (6), discriminant function g_1 is primarily influenced by the control common factor, speed common factor, and driver response common factor. In contrast, discriminant function g_2 is mainly affected by driver gender, the control common factor, and the speed factor.

To intuitively demonstrate the performance of the driver avoidance capability discrimination model, Figure 11 presents the joint distribution scatter plot of the three driver categories, with the first and second discriminant functions serving as the two coordinate axes. As shown in Figure 11, the three categories are clearly separated from each other, indicating that the developed model provides effective discrimination among different avoidance capability levels. For a driver whose avoidance capability category needs to be classified, the corresponding discriminant scores can be calculated and projected onto the joint distribution space. The observation can then be assigned to the category with the nearest group centroid based on the distance between the point and the centroids of the predefined groups.

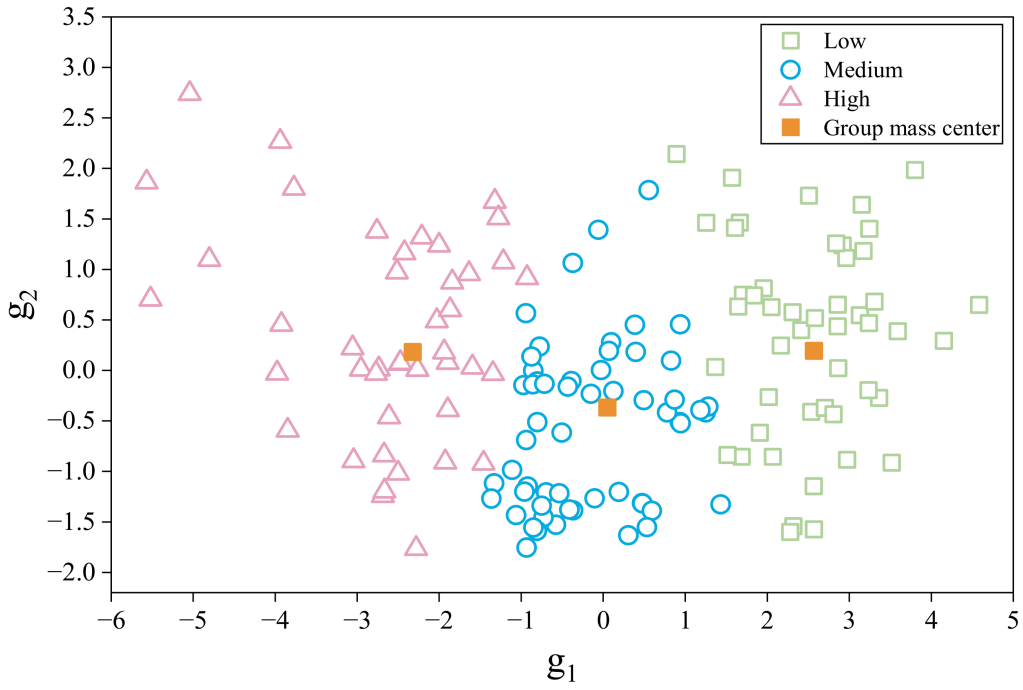


Figure 11. Scatter plot of the joint distribution of driver avoidance capability.

To achieve effective classification of driver avoidance capability levels, Bayesian linear discriminant functions were employed to classify the sample categories. Table 5 presents the coefficients of the discriminant functions, where the number of discriminant functions corresponds to the number of driver avoidance capability categories. By substituting the observed values of the variables for a sample into the discriminant functions given in Equation (7), three discriminant scores can be obtained. The sample is then assigned to the corresponding avoidance capability category according to the maximum discriminant score criterion, whereby the category associated with the largest discriminant function value is selected.

$$\begin{cases} Y_1 = 6.714x_1 + 6.326x_2 + 3.082F_1 + 3.024F_2 + 5.661F_3 - 14.299 \\ Y_2 = 5.647x_1 + 6.383x_2 + 0.550F_1 + 0.537F_2 + 1.263F_3 - 9.631 \\ Y_3 = 5.786x_1 + 6.529x_2 - 0.921F_1 - 2.058F_2 - 3.108F_3 - 12.689 \end{cases} \quad (7)$$

where Y_1, Y_2, and Y_3 represent low, medium, and high avoidance capability levels, respectively. The meanings of the independent variables are consistent with those defined in Equation (6).

Table 5. Coefficients of Bayesian linear discriminant functions.

Variable	Gender	Hazard Visibility	F1	F2	F3	Constant
Y1	6.714	6.326	3.082	3.024	5.661	−14.299
Y2	5.647	6.383	0.550	0.537	1.263	−9.631
Y3	5.786	6.529	−0.921	−2.058	−3.108	−12.689

The classification results of the driver avoidance capability discrimination model are presented in Table 6. In the original group, there were 46 samples in the low avoidance capability group, 50 samples in the medium avoidance capability group, and 52 samples in the high avoidance capability group. The results show that 95.65% of the samples in the low avoidance capability group were correctly classified, while 4.35% were misclassified into the medium avoidance capability group. The classification performance of the other capability groups followed a similar pattern. Overall, the proposed model correctly classified 85.8% of the samples, demonstrating its effectiveness in identifying drivers with different avoidance capability levels.

Table 6. Classification results.

Case Clustering		Prediction Group Member			
		Low	Medium	High	Total
Original group member	Low	95.65%	4.35%	0.00%	100.0%
	Medium	8.00%	86.00%	6.00%	100.0%
	High	0.00%	23.08%	76.92%	100.0%

Table 5 presents the coefficients of the Bayesian linear discriminant functions based on gender, hazard visibility, and the three behavioral factors: F1, F2, and F3. The coefficients of these factors varied across the three discriminant functions, indicating that the observed differences among the TTC-defined groups were characterized by different combinations of vehicle control, speed-related characteristics, and driver response. Gender and hazard visibility also contributed to the discriminant functions, indicating that individual characteristics and hazard visibility were associated with the observed response-pattern differences. Given that the avoidance-capability groups were defined based on TTC, these discriminant functions are interpreted as an exploratory characterization of the response patterns observed in the three TTC-defined groups, rather than as an independent predictive model for classifying new drivers.

4. Discussion

This study designed driving simulation experiments under different risk scenarios to collect drivers' braking responses and behavioral characteristic parameters. The differential effects of hazard visibility and driver gender on avoidance behaviors were investigated. Furthermore, factor analysis and Bayesian linear discriminant analysis were integrated to develop a driver avoidance capability discrimination model, enabling the quantitative classification of drivers' avoidance capability levels.

The multidimensional analysis of BPF, Max BPF, acceleration, maximum deceleration, speed, initial braking speed, BRT, and BRP demonstrated that hazard visibility is a dominant factor influencing drivers' avoidance behaviors and overall avoidance capability, with a stronger effect than individual gender differences. Compared with overt hazard conditions, covert hazards substantially altered drivers' avoidance strategies. In terms of vehicle motion characteristics, covert hazards significantly increased drivers' maximum braking pedal force ($F = 5.254$, $p = 0.024 < 0.05$), suggesting that when drivers fail to perceive potential hazards in advance, they tend to adopt more aggressive and high-intensity emergency braking strategies to compensate for insufficient hazard anticipation. Furthermore, drivers under covert hazard conditions exhibited larger BRP values, indicating that braking was initiated at a later stage with reduced available distance before the potential conflict point. The TTC analysis further confirmed this pattern, showing that covert hazards substantially reduced drivers' temporal safety margins and resulted in significantly elevated collision risk levels. In summary, overt hazards provide drivers with sufficient time and space for hazard perception, risk anticipation, and gradual speed adjustment. In contrast, covert hazards are associated with delayed hazard recognition, forcing drivers to rely on high-intensity emergency braking as a compensatory response. Consequently, avoidance maneuvers under covert hazard conditions impose greater operational demands on drivers and result in reduced safety margins. These findings are consistent with previous studies demonstrating that sudden and concealed roadway hazards increase driver workload and elevate crash risk. Furthermore, the results provide further insights into the underlying mechanisms contributing to the higher crash incidence associated with visually occluded risks, such as vehicle obstruction at intersections and unexpected pedestrian emergence from roadside areas.

For covert hazards, it is worth noting that BRT is initiated at the trigger point 80 m upstream of the conflict point and includes the period before the hazard becomes visible to drivers; this interval is longer by experimental design, meaning the observed BRT differences between covert and overt hazards may be partially definitional and not solely driven by driver hazard perception. In such covert hazard scenarios, hazards are temporarily hidden from drivers' view, and even when drivers visually scan the scene, they may still fail to detect hidden road users and commit "looked but failed to see" errors. This phenomenon has been well documented in previous studies examining visual scanning patterns and perceptual failures at occluded intersections [35,36]. Therefore, the longer BRT observed for covert hazards may partly reflect both the definitional effect of the measurement setup and the extra cognitive demand associated with searching for occluded hazards, together with the risk of perceptual omission.

The influence of driver gender on avoidance capability does not follow a single consistent pattern but exhibits strong scenario-dependent characteristics, resulting in differentiated behavioral responses under overt and covert hazard conditions. Overall, male drivers demonstrated more intensive braking control behaviors under covert hazard conditions. This finding suggests that male drivers tend to adopt rapid and more aggressive vehicle control strategies when encountering sudden hazards, reducing collision risk by applying stronger braking inputs [37]. Such behavioral tendencies may be associated with higher

levels of driving confidence and greater risk-taking propensity among male drivers. In contrast, female drivers generally exhibited smoother braking behaviors, with relatively smaller variations in deceleration and braking force. Although female drivers sometimes adopted lower-intensity braking maneuvers, their vehicle control processes were more continuous and stable, potentially reducing fluctuations in vehicle dynamics caused by excessive braking.

As a representative surrogate safety measure, TTC can effectively characterize the remaining safety margin during hazardous interactions [38]. As shown in Figure 8, significant differences in TTC distributions were observed between different hazard visibility conditions ($F(1,148) = 15.362$, $p < 0.01$). Compared with overt hazard conditions, covert hazards resulted in an overall reduction in TTC, indicating a higher collision risk under scenarios with limited hazard visibility. This phenomenon can be primarily attributed to the reduced effective perception time caused by covert hazards, which shortens the available response window before vehicles enter critical conflict states. This finding suggests that enhanced vehicle control can only partially mitigate collision risk and cannot fully compensate for the safety loss induced by delayed hazard recognition [39]. During the period when the driver is delayed in perceiving the risk, the vehicle continues to move forward at the original speed. The distance traveled during this period will not be eliminated by subsequent stronger braking operations; even if the driver can quickly apply greater braking pedal force and achieve a higher deceleration rate later, it can only shorten the braking distance required during the deceleration phase, but the perception delay has already consumed the limited TTC in the conflict scenario, compressing the overall risk avoidance time window. Therefore, for sudden hazard events, improving drivers' emergency braking capability alone is insufficient to effectively reduce crash risk. More importantly, enhancing early hazard perception and risk warning mechanisms is essential for extending drivers' available response time and improving overall traffic safety.

This study has several limitations. Firstly, all participants completed the conflict scenarios in the same fixed order. This design may introduce learning or fatigue effects. Secondly, the sample size in this study was relatively limited, and the demographic characteristics of participants, such as age and driving experience, covered a restricted range. Thirdly, a total of nine statistical tests were performed in this study. These tests are not fully independent because they are derived from the same set of driving conflict observations. We did not apply multiple-testing correction (e.g., Bonferroni or FDR correction) to these tests. Consequently, the familywise Type I error rate may be inflated. Future research should recruit a larger and more diverse driver population and incorporate additional individual characteristics to improve the robustness and generalization capability of the discrimination model. Furthermore, the avoidance behaviors and underlying mechanisms associated with hazard visibility in more complex traffic scenarios, such as lane-changing interactions and intersection conflicts, require further investigation.

5. Conclusions

This study developed driving simulation scenarios with different levels of hazard visibility and collected drivers' avoidance behavior data under various risk conditions. Based on TTC, driving risk was classified into three levels: low, medium, and high. Subsequently, factor analysis and Bayesian linear discriminant analysis were integrated to establish a driver avoidance capability classification model. The main findings of this study are summarized as follows:

(1) Hazard visibility had a significant effect on the Max BPF ($F = 5.254$, $p = 0.024 < 0.05$). Drivers under covert hazard conditions exhibited significantly greater Max BPF than those under overt hazard conditions, with a mean difference of 3.186 daN. In addition,

hazard visibility significantly influenced the BRP ($F = 8.895$, $p < 0.01$). The BRP of drivers under covert hazard conditions was larger than that under overt hazard conditions, with a mean difference of 11.762 m. Drivers with higher avoidance capability exhibited distinct behavioral characteristics across multiple dimensions. In terms of vehicle control behavior, stronger avoidance capability was associated with lower BPF, Max BPF, and maximum deceleration, and tended to maintain lower speed and smaller acceleration variations. In terms of response behavior, it is indicated by BRT and BRP being smaller, suggesting that the driver takes braking measures when the distance to the potential collision conflict location is relatively far and has a shorter reaction time.

(2) Factor analysis was applied to reduce the dimensionality of eight behavioral indicators, including BPF, Max BPF, acceleration, maximum deceleration, speed, initial braking speed, BRT, and BRP. Three common factors were extracted, accounting for 86.68% of the cumulative variance. This dimensionality reduction effectively addressed the multicollinearity among the original variables while preserving the essential information underlying drivers' avoidance behaviors. The Bayesian linear discriminant model developed based on the extracted factors achieved an overall classification accuracy of 85.8% for driver avoidance capability identification.

The findings of this study provide theoretical insights into understanding drivers' avoidance behaviors from the perspective of hazard visibility. Moreover, the proposed approach offers methodological support and decision-making references for the quantitative assessment of drivers' risk perception and avoidance capability, the development of hierarchical driver training programs, and the optimization of warning strategies in intelligent driver assistance systems.

Author Contributions: The authors confirm contribution to the paper as follows: study conception and design: J.Z., Y.H. and T.W.; data collection: Y.H. and T.W.; analysis and interpretation of results: J.Z.; draft manuscript preparation: J.Z. and T.W. All authors have read and agreed to the published version of the manuscript.

Funding: This research was funded by Shandong Provincial Natural Science Foundation project (ZR2025QC741) and the Innovative Team Project of Ji'nan Government (202333036).

Institutional Review Board Statement: This study is waived for ethical review as Article 32 of the Measures for the Ethical Review of Research Involving Human Life Sciences and Medicine (Document No. Guo Wei Ke Jiao Fa [2023] 4), by the Ethics Committee of Shandong Jiaotong University, Ji'nan, China.

Informed Consent Statement: Informed consent was obtained from all subjects involved in the study.

Data Availability Statement: The data used to support the findings of this study are available from the corresponding author upon request.

Conflicts of Interest: The authors declare no conflicts of interest.

Abbreviations

The following abbreviations are used in this manuscript:

BPF	Brake Pedal Force
BRP	Braking Response Position
BRT	Brake Reaction Time
KMO	Kaiser Meyer Olkin
LMM	Linear Mixed Model
Max BPF	Maximum Brake Pedal Force
SSM	Surrogate Safety Measures
TTC	Time To Collision
V-V	Vehicle–Vehicle Conflicts

V-C	Vehicle–Cycle Conflicts
V-P	Vehicle–Pedestrian Conflicts

References

1. Guo, W.; Xu, W.; Yang, C.; Zhao, Z.; Gao, X.; Yao, W.; Jin, S. CRFPI-Net: Context-aware risk feature perception and inference network for pixel-level urban traffic risk mapping. *Adv. Eng. Inform.* **2026**, *71*, 104299. [CrossRef]
2. Khattak, A.J.; Ahmad, N.; Wali, B.; Dumbaugh, E. A taxonomy of driving errors and violations: Evidence from the naturalistic driving study. *Accid. Anal. Prev.* **2021**, *151*, 105873. [CrossRef] [PubMed]
3. Zarei, A.H.; Asadamraji, M. Hazard perception and prediction model based on cognitive components of male BRT drivers. *Traffic Inj. Prev.* **2026**, 1–9. [CrossRef] [PubMed]
4. Horswill, M.S.; Hill, A.; Jackson, T. Scores on a new hazard prediction test are associated with both driver experience and crash involvement. *Transp. Res. Part F Traffic Psychol. Behav.* **2020**, *71*, 98–109. [CrossRef]
5. Ou, Y.-K.; Chen, W.-R.; Fang, C.-W. Gaze tracking patterns on different types of traffic risk in early-stage Alzheimer's disease. *Transp. Res. Part F Traffic Psychol. Behav.* **2022**, *91*, 451–460. [CrossRef]
6. Wen, J.; Lyu, N. Risk characteristics analysis of road segments: Considering multiple scales and temporal stages. *Traffic Inj. Prev.* **2025**, *26*, 998–1008. [CrossRef] [PubMed]
7. Su, S.; Chen, H.; Yang, J.; Xia, T.; Guo, C.; Yin, Y. Study on modeling driver subjective risk perception in dynamic curve driving condition. *Proc. Inst. Mech. Eng. Part D. J. Automob. Eng.* **2025**, 09544070251410645. [CrossRef]
8. Machado-León, J.L.; de Oña, J.; de Oña, R.; Eboli, L.; Mazzulla, G. Socio-economic and driving experience factors affecting drivers' perceptions of traffic crash risk. *Transp. Res. Part F Traffic Psychol. Behav.* **2016**, *37*, 41–51. [CrossRef]
9. Guo, M.; Zhao, X.; Yao, Y.; Yang, H.; Qi, J.; Su, Y. Investigating the impacts of driver's risky driving behavior on traffic crash risk detection model. *J. Transp. Saf. Secur.* **2024**, *16*, 130–156. [CrossRef]
10. Chen, S.; Cheng, K.; Yang, J.; Zang, X.; Luo, Q.; Li, J. Driving behavior risk measurement and cluster analysis driven by vehicle trajectory data. *Appl. Sci.* **2023**, *13*, 5675. [CrossRef]
11. Lee, M.; Kim, S.; Kim, J.; Yang, J.H. Simulator study on the response time and defensive behavior of drivers in a cut-in situation. *Int. J. Automot. Technol.* **2022**, *23*, 817–827. [CrossRef]
12. Johnsson, C.; Laureshyn, A.; De Ceunynck, T. In search of surrogate safety indicators for vulnerable road users: A review of surrogate safety indicators. *Transp. Rev.* **2018**, *38*, 765–785. [CrossRef]
13. Yin, Y.; Zhang, Y.; Xu, Y.; Huang, W. A human-centered risk pulse field framework for real-time car-following risk control in connected driving environments. *Accid. Anal. Prev.* **2026**, *236*, 108674. [CrossRef] [PubMed]
14. Yan, Z.; Saunier, N.; Yue, L.; Sun, J. Investigating and modeling crash risk for interactions between motorized and non-motorized in intersection center areas. *Traffic Inj. Prev.* **2025**, *26*, 686–696. [CrossRef] [PubMed]
15. Ge, H.; Huang, M.; Lu, Y.; Yang, Y. Study on traffic conflict prediction model of closed lanes on the outside of expressway. *Symmetry* **2020**, *12*, 926. [CrossRef]
16. Torkashvand, M.B.; Aghayan, I.; Qin, X.; Hadadi, F. An extended dynamic probabilistic risk approach based on a surrogate safety measure for rear-end collisions on two-lane roads. *Phys. A Stat. Mech. Its Appl.* **2022**, *603*, 127845. [CrossRef]
17. Liu, C.; Nacpil, E.J.C.; Wang, Z.; Guan, H.; Hou, W.; Zheng, R. Investigation of luminance influence on driver risk perception according to visual time-to-collision. *Transp. Res. Part F Traffic Psychol. Behav.* **2026**, *119*, 103597. [CrossRef]
18. Lee, D.N. A theory of visual control of braking based on information about time-to-collision. *Perception* **1976**, *5*, 437–459. [CrossRef] [PubMed]
19. Sun, L.; Zhang, M.; Qiu, Y.; Zhang, C. Effects of sleep deprivation and hazard types on the visual search patterns and hazard response times of taxi drivers. *Behav. Sci.* **2023**, *13*, 1005. [CrossRef] [PubMed]
20. Huang, W.-C.; Fan, L.-H.; Han, Z.-J.; Niu, Y.-F. Enhancing safety in conditionally automated driving: Can more takeover request visual information make a difference in hazard scenarios with varied hazard visibility? *Accid. Anal. Prev.* **2024**, *205*, 107687. [CrossRef] [PubMed]
21. Baikejuli, M.; Li, R. Analysis of multi-factor coupling mechanisms of truck drivers' aberrant driving behaviors. *Accid. Anal. Prev.* **2026**, *236*, 108666. [CrossRef] [PubMed]
22. Peng, Y.; Cheng, L.; Jiang, Y.; Zhu, S. Examining Bayesian network modeling in identification of dangerous driving behavior. *PLoS ONE* **2021**, *16*, e0252484. [CrossRef] [PubMed]
23. Fernandez, S.; Ito, T.; Cruz-Piris, L.; Marsa-Maestre, I. Fuzzy ontology-based system for driver behavior classification. *Sensors* **2022**, *22*, 7954. [CrossRef] [PubMed]
24. Pourghasemi, M.; Rezaei, E.; Ansariyar, A.; Ardeshiri, A.; Jeihani, M.; Tootkaboni, M. Driving behavior recognition and scoring: A Bayesian approach to driving simulator data analytics. *Accid. Anal. Prev.* **2026**, *232*, 108523. [CrossRef]

25. Sullman, M.J.; Stephens, A.N.; Taylor, J.E. Dimensions of aberrant driving behaviour and their relation to crash involvement for drivers in New Zealand. *Transp. Res. Part F Traffic Psychol. Behav.* **2019**, *66*, 111–121. [CrossRef]
26. Yang, L.; Li, X.; Guan, W.; Jiang, S. Assessing the relationship between driving skill, driving behavior and driving aggressiveness. *J. Transp. Saf. Secur.* **2022**, *14*, 737–753. [CrossRef]
27. Javid, M.A.; Al-Hashimi, A.R. Significance of attitudes, passion and cultural factors in driver's speeding behavior in Oman: Application of theory of planned behavior. *Int. J. Inj. Control Saf. Promot.* **2020**, *27*, 172–180. [CrossRef] [PubMed]
28. Wang, Y.; Wang, L.; Zhu, R.; Xu, Y.; Jiang, G.; Ma, X. Conflict judgment and safety assessment at unsignalized intersections based on machine vision. *J. Adv. Transp.* **2023**, *2023*, 6465225. [CrossRef]
29. Li, H.; Zheng, T.; Xia, F.; Gao, L.; Ye, Q.; Guo, Z. Emergency collision avoidance strategy for autonomous vehicles based on steering and differential braking. *Sci. Rep.* **2022**, *12*, 22647. [CrossRef] [PubMed]
30. Jiang, H.; Deng, H. Traffic incident detection method based on factor analysis and weighted random forest. *IEEE Access.* **2020**, *8*, 168394–168404. [CrossRef]
31. Amrapala, C.; Choocharukul, K. Exploring relationship between perceived risk and risky driving behavior of motorcyclists in Bangkok, Thailand. *Transp. Res. Interdiscip. Perspect.* **2025**, *34*, 101628. [CrossRef]
32. Xue, Q.; Wang, K.; Lu, J.J.; Liu, Y. Rapid Driving Style Recognition in Car-Following Using Machine Learning and Vehicle Trajectory Data. *J. Adv. Transp.* **2019**, *1*, 9085238. [CrossRef]
33. Wang, W.; Yuan, M. Risk-Avoidance Driving Style Identification and Risk Influencing Factors Based on Improved CatBoost. *Highw. Automot. Appl.* **2026**, *42*, 17–23. [CrossRef]
34. Wang, J.; Zhang, X.; Chang, X.; Zhou, Z.; Wang, C.; Fu, Z.; Fu, B. Prediction model for blast-induced structural damage based on an optimized Bayes discriminant analysis model. *Appl. Math. Model.* **2022**, *110*, 338–366. [CrossRef]
35. Langham, M.; Hole, G.; Edwards, J.; O'Neil, C. An analysis of'looked but failed to see'accidents involving parked police vehicles. *Ergonomics* **2002**, *45*, 167–185. [CrossRef] [PubMed]
36. Brown, L.; Morris, A.; Thomas, P.; Ekambaram, K.; Margaritis, D.; Davidse, R.; Usami, D.S.; Robibaro, M.; Persia, L.; Buttler, I.; et al. Investigation of accidents involving powered two wheelers and bicycles–A European in-depth study. *J. Saf. Res.* **2021**, *76*, 135–145. [CrossRef] [PubMed]
37. Pawar, N.M.; Khanuja, R.K.; Choudhary, P.; Velaga, N.R. Modelling braking behaviour and accident probability of drivers under increasing time pressure conditions. *Accid. Anal. Prev.* **2020**, *136*, 105401. [CrossRef] [PubMed]
38. Wang, S.; Jiang, J.; Li, Z.; Liu, Z.; Zhao, W.; Li, P.; Zhang, G.; Ou, S. Safety-to-trust dynamics: Can automated vehicles navigate yellow-light dilemma zones from the driver's perspective? *Accid. Anal. Prev.* **2026**, *233*, 108587. [CrossRef] [PubMed]
39. Bella, F.; Silvestri, M. Effects of directional auditory and visual warnings at intersections on reaction times and speed reduction times. *Transp. Res. Part F Traffic Psychol. Behav.* **2017**, *51*, 88–102. [CrossRef]

Disclaimer/Publisher's Note: The statements, opinions and data contained in all publications are solely those of the individual author(s) and contributor(s) and not of MDPI and/or the editor(s). MDPI and/or the editor(s) disclaim responsibility for any injury to people or property resulting from any ideas, methods, instructions or products referred to in the content.